

Taylor & Francis
Taylor & Francis Group

Science and Technology of Advanced Materials: Methods

ISSN: 2766-0400 (Online) Journal homepage: www.tandfonline.com/journals/tstm20

Luminance histogram analysis for RHEED images using peak fitting approach with machine learning technique

Asako Yoshinari, Yasunobu Ando, Tarojiro Matsumura, Masato Kotsugi, Shuji Hasegawa, Rei Hobara & Naoka Nagamura

To cite this article: Asako Yoshinari, Yasunobu Ando, Tarojiro Matsumura, Masato Kotsugi, Shuji Hasegawa, Rei Hobara & Naoka Nagamura (2026) Luminance histogram analysis for RHEED images using peak fitting approach with machine learning technique, Science and Technology of Advanced Materials: Methods, 6:1, 2666924, DOI: 10.1080/27660400.2026.2666924

To link to this article: https://doi.org/10.1080/27660400.2026.2666924

© 2026 The Author(s). Published by National Institute for Materials Science in partnership with Taylor & Francis Group

View supplementary material

Published online: 04 Jun 2026.

Submit your article to this journal

Article views: 581

View related articles

View Crossmark data

Full Terms & Conditions of access and use can be found at
https://www.tandfonline.com/action/journalInformation?journalCode=tstm20

SCIENCE AND TECHNOLOGY OF ADVANCED MATERIALS: METHODS
2026, VOL. 6, NO. 1, 2666924
https://doi.org/10.1080/27660400.2026.2666924

Taylor & Francis
by informa

OPEN ACCESS Check for updates

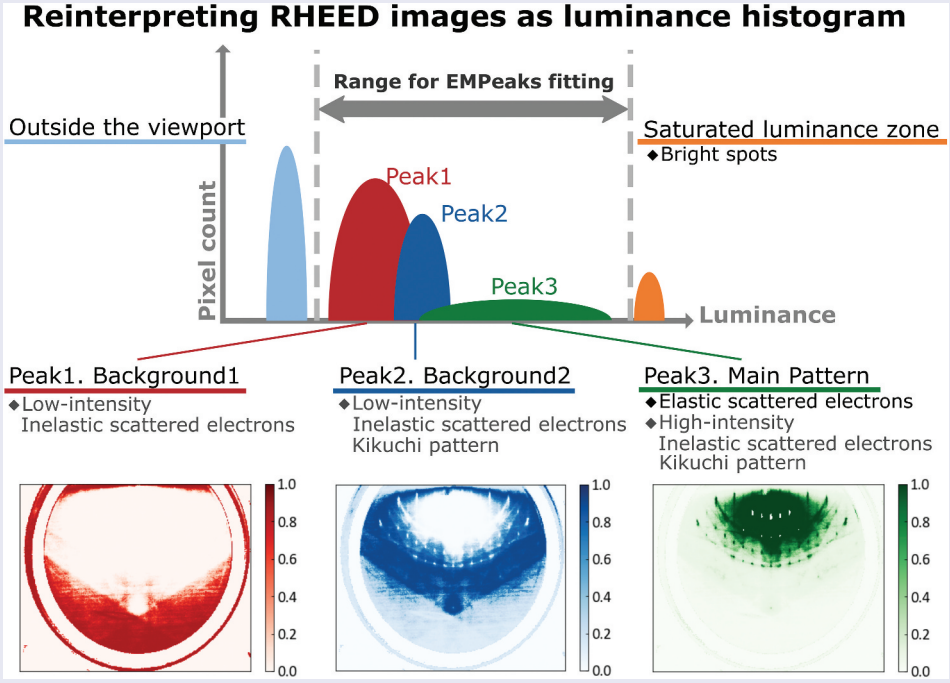
Luminance histogram analysis for RHEED images using peak fitting approach with machine learning technique

Asako Yoshinari [a,b], Yasunobu Ando [c], Tarojiro Matsumura [d], Masato Kotsugi [a], Shuji Hasegawa [e], Rei Hobara [e] and Naoka Nagamura [a,b]

[a]Graduate School of Department of Materials Science and Technology, Tokyo University of Science, Tokyo, Japan; [b]Center for Basic Research on Materials, National Institute for Materials Science (NIMS), Tsukuba, Japan; [c]Laboratory for Chemistry and Life Science, Institute of Integrated Research, Institute of Science Tokyo, Tokyo, Japan; [d]Materials DX Research Center, National Institute of Advanced Industrial Science and Technology(AIST), Tsukuba, Japan; [e]Graduate School of Science Department of Physics, The University of Tokyo, Tokyo, Japan

ABSTRACT

Reflection high-energy electron diffraction (RHEED) is widely used for *in situ* observation during physical vapor deposition (PVD) processes such as molecular beam epitaxy (MBE) to precisely control of the two-dimensional materials fabrication, which is promising for next-generation electronic devices. Although automatic analysis using machine learning technique has been attracting for taking in the abundant information contained in RHEED, there are still problems such as the robustness of image misalignment or the possibility of *in situ* analysis. In this study, we propose an automatic analysis method based on a luminance-histogram representation of RHEED images, in which the histogram is treated as a spectrum and analyzed using a high-throughput peak fitting technique. The method is robust to image misalignment and has *in situ* analysis possibility. Applied to RHEED images of the indium deposition process on to Si(111) surface, we achieved to estimate the optimal deposition time for fabricating each surface superstructure and the external parameter changing time.



IMPACT STATEMENT

By reinterpreting RHEED patterns as spectral luminance histograms, this study establishes a high-speed data-driven framework for monitoring structural phase transitions. The method's computational efficiency and resilience to image shifts pave the way for real-time, autonomous process control in next-generation material fabrication.

ARTICLE HISTORY
Received 19 February 2026
Revised 21 April 2026
Accepted 26 April 2026

KEYWORDS
RHEED; machine learning; PVD; *in situ* analysis; luminance histgram

CONTACT Asako Yoshinari 8223702@ed.tus.ac.jp Graduate School of Department of Materials Science and Technology, Tokyo University of Science, 6-3-1 Niijuku, Katsushika-ku, Tokyo 125-8585, Japan; Yasunobu Ando yasunobu.ando@cls.iir.isct.ac.jp Laboratory for Chemistry and Life Science, Institute of Integrated Research, Institute of Science Tokyo, 4259 Nagatsuta-cho, Midori-ku, Yokohama, Kanagawa 226-8501, Japan; Naoka Nagamura NAGAMURA.Naoka@nims.go.jp Center for Basic Research on Materials, National Institute for Materials Science, 3-13 Sakura, Tsukuba, Ibaraki 305-0003, Japan

Supplemental data for this article can be accessed online at https://doi.org/10.1080/27660400.2026.2666924

© 2026 The Author(s). Published by National Institute for Materials Science in partnership with Taylor & Francis Group
This is an Open Access article distributed under the terms of the Creative Commons Attribution License (http://creativecommons.org/licenses/by/4.0/), which permits unrestricted use, distribution, and reproduction in any medium, provided the original work is properly cited. The terms on which this article has been published allow the posting of the Accepted Manuscript in a repository by the author(s) or with their consent.

1. Introduction

Starting with graphene, transition metal dichalcogenides, borophene, and silicene, the creation of various two-dimensional materials [1–4] and the exploration or evaluation of their electronic properties, such as optical, electrical, and topological properties [1–4], have attracted much attention and research. Physical vapor deposition (PVD) processes such as molecular beam epitaxy (MBE) are often applied for the precise fabrication of such two-dimensional materials, and reflection high-energy electron diffraction (RHEED) is widely used for *in situ* observation to characterize their structures.

RHEED provides many kinds of patterns that contain various information, such as periodic information of the surface structure, lattice constant, crystallinity, substrate temperature, and intensity of incident electron beams [5–10], but the abundant information is not fully utilized because theoretical calculation or quantitative interpretation of spot intensity is difficult due to complex diffraction process. For example, RHEED intensity oscillation is a common indicator for estimating film thickness from the period of oscillation. Conventionally, experimenters focus on selected spot intensity during deposition. However, as mentioned above, RHEED contains complex information other than film thickness, so using only a part of the information in a personalized way is not accurate. Therefore, it is expected that information such as intensity oscillation or growth mode can be extracted from the whole RHEED image by analysis using machine learning, and machine learning analysis of RHEED images has begun to attract attention in recent years [11–25].

The Si(111) surface is a prototypical model system that exhibits a variety of surface reconstructions depending on the adsorbed atoms, and it plays an important role in the study of surface physics and low-dimensional electronic systems. In particular, for the indium-adsorbed system, multiple stable surface superstructures emerge depending on the deposition amount [4], each exhibiting markedly different electronic states and physical properties. These structural transitions can be observed *in situ* by RHEED, making it an indispensable technique for understanding and controlling growth processes.

In our previous study, we applied several unsupervised learning methods to RHEED images of indium (In) adsorption processes on Si(111) surfaces, and were able to automatically detect changes in surface superstructures by hierarchical clustering and to automatically estimate the optimal deposition time to fabricate each surface superstructure by non-negative matrix factorization [11]. However, some problems remain in the analysis of RHEED images using machine learning [11], the one-dimensional array of image luminance is used as the feature value. First, the analysis is not robust to image misalignment, second, it is difficult to find important features in the MBE process in high-dimensional RHEED images, and last, analysis can be performed only after the images are taken.

In this study, we introduce a data-driven approach that focuses on the statistical luminance distribution of the RHEED information, eliminating dependency on operator skill. In this method, RHEED images are transformed into luminance histograms and analyzed as spectra, offering a new perspective distinct from traditional spatial tracking. This approach takes advantage of the fact that surface structural evolutions are intrinsically reflected in the variation of diffraction intensities. Consequently, this spectral treatment allows for the high-throughput detection of surface condition changes and the extraction of hidden information through machine learning algorithms.

In relation to the spectrum analysis, we employed 'EMPeaks', a package for high-throughput peak fitting analysis of large amounts of spectral data using machine learning [26–29]. The method is based on the expectation-maximization (EM) algorithm that is one of the algorithm for maximum likelihood estimation (MLE) by iterative computation of the parameters of an assumed mixture distribution model. We note that this method is fast, robust to noise and initial guess for parameters to some extent, and *in situ* analysis possibility, which is promising to solve the previous problem. Therefore, we came up with applying high-throughput peak fitting analysis method using EMPeaks to luminance histogram spectrums.

2. Results and discussion

In the development, we used a RHEED image dataset obtained by resistively heating a Si(111)-7×7 clean surface while depositing indium [9–11,30], observing five stages of change: 7×7 clean surface, $\sqrt{3} \times \sqrt{3}$ structure, $\sqrt{31} \times \sqrt{31}$ structure, 4×1 structure and 4×1 structure after the current heating stopped. Each image was converted to a luminance histogram and considered as a spectrum. Representative RHEED images and histograms are presented in Figure 1. By applying high-throughput peak fitting analysis using EMPeaks to the luminance histograms, we propose a totally new analysis idea that uses the entire πinto three elements on the luminance histogram [26–29]. By following the time series changes in some parameters, the optimal deposition time to fabricate each structure can be estimated, as well as external parameters change times such as deposition stop and heating stop. The proposed method is robust against image misalignment and is expected to be a new method with the potential for *in situ* analysis.

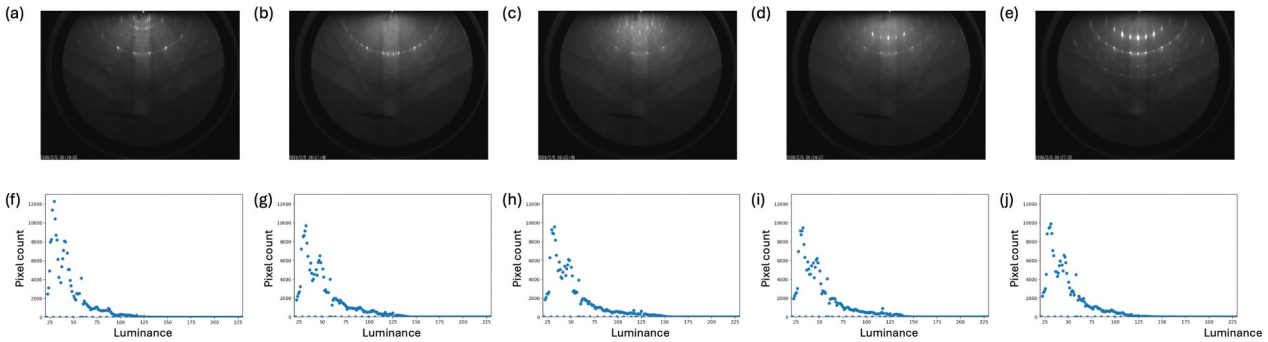


Figure 1. The original RHEED images used for analysis, selected as representative for each structure, and their histograms; (a)(f) 7×7 (1st image, corresponding to 0 s), (b)(g) $\sqrt{3}\times\sqrt{3}$ (104th image, corresponding to 132 s), (c)(h) $\sqrt{31}\times\sqrt{31}$ (150th image, corresponding to 190 s), (d)(i) 4×1 (230th image, corresponding to 292 s), (e)(j) 4×1 w/o annealing after stopping deposition (375th image, corresponding to 480 s).

The substrate was an n-type (resistivity of 1–10 Ω·cm at 300 K) Si(111) wafer with a 1.8° miscut along the $[1\bar{1}\bar{2}]$ direction for single-domain 4×1-In chains, and the size was 3 mm × 10 mm. The substrate was direct current (DC) heated for a few seconds at 1200 °C under an ultrahigh vacuum (UHV) chamber ($\sim10^{-8}$ Pa) to remove oxide layer, and then annealed at 1050 °C to produce terrace with one atom high steps and at 850 °C to form Si(111)-7×7 surface superstructure. Next, indium was deposited by molecular beam epitaxy (MBE) on the Si substrate at 450 °C with DC heating. At the same time as the deposition started, recording of RHEED pattern images started using a charge-coupled device (CCD) camera. The shutter of the indium source was closed at 392 s, the DC heating was finished at 421 s, and the RHEED pattern observation was completed at 480 s later. The average interval between image taking was 1.28 s and a total of 375 RHEED images were obtained. The size of RHEED pattern images was 480×640 (h × w) pixels, and the RHEED conditions were acceleration voltage 15 kV, beam current 36 μA, incident angle 3.0° and incident azimuth $[112^{-}]$ [7–10]. A histogram was generated for each of the 375 RHEED images obtained by counting the number of pixels from 0 to 255 luminance. The obtained histograms were considered as spectrum, and peak fitting was performed using EMPeaks [26–29]. The fitting conditions were as follows: a Gaussian mixture model with three components are used to characterize the luminance histograms, the fitting range was 20–220 luminance, the initial value of each mean value was randomly set, and 5 fitting trials were performed for a single spectrum, or luminance histogram. Note that fitting with EMPeaks can lead to not a global solution but local solutions, so if the results do not converge well with random initial values or a small number of trials, it is necessary to find the optimal initial values and number of trials. In the EMPeaks approach employed in this study, several parameters must be empirically set as initial conditions. Although such settings are currently required, extended versions of EMPeaks have been proposed to reduce the influence of initial conditions and thereby improve analytical efficiency [29]. Whereas applications to RHEED data have been at an early stage, these methods represent a promising way for efficiently analyzing. Data analysis was performed using the following machine learning software and libraries: Python (Version: 3.7.6), EMPeaks (Version: 2.0.2). The computer used for the analysis was equipped with an Intel(R) Core(TM) i5 CPU with four cores at 1.60 GHz and 16 GB memory.

The diffraction pattern of the obtained RHEED image clearly changes in several steps even by visual inspection. Together with the phase diagram [4,9] and our previous study [11], the structure is confirmed to be 7×7, $\sqrt{3}\times\sqrt{3}$, $\sqrt{31}\times\sqrt{31}$, 4×1, and 4×1 after stopping DC heating.

The first and 375th luminance histograms (first image & last image) of RHEED pattern in the MBE process obtained by counting the number of pixels with each luminance in the image are shown in Figure 2(a,b). In the low luminance side and high luminance side, there is irregularly high pixel count (the high luminance range is a little difficult to see), and two sharp peaks and one gentle peak, totaling three peaks appear in the middle range. Binarization and visualization of the low and high luminance ranges (Figure 2(c,d)) confirmed that they are outside the viewport and the area where the diffraction spot intensity is strong and saturated with luminance, respectively. To reduce the convergence of the fitting, the range of 20–220 was set as the range to be fitted by EMPeaks, and the number of peaks was determined to be three. However, since the pixels in the high-luminance side contain important RHEED information as diffraction spots, the information is extracted later by counting the sum of luminance. The histograms of all the images will be placed in Supplement as a movie. As a precaution, it is necessary to check the actual shape of the obtained histogram to determine the number of peaks. In this case, the high luminance

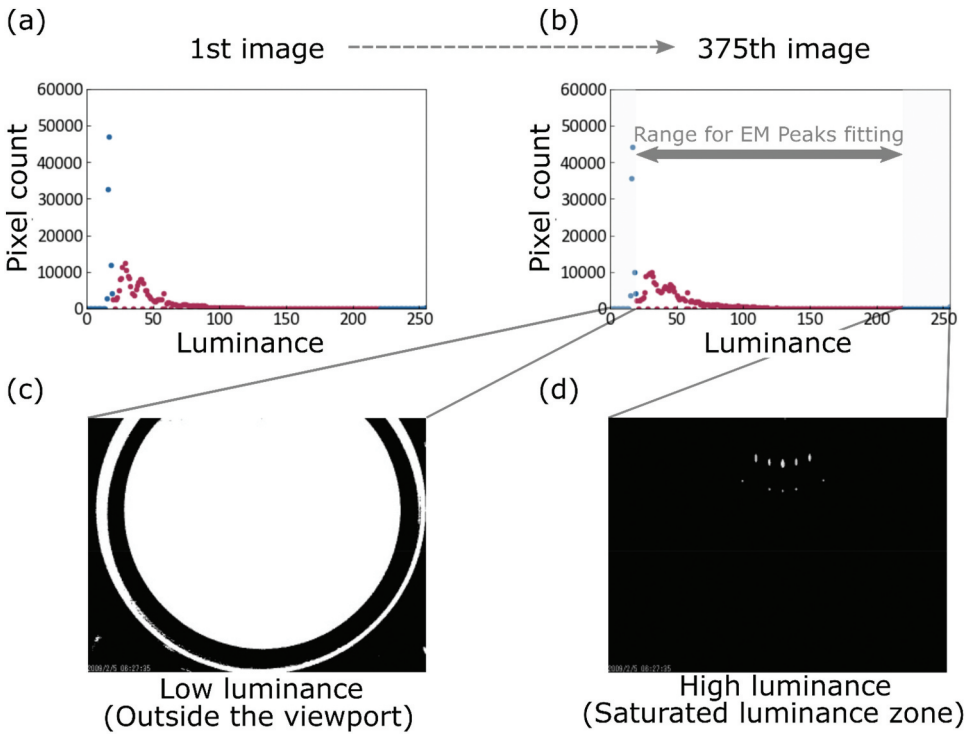


Figure 2. Results of luminance histogram (a, b) luminance histogram of first image and 375th (last) image. Unnaturally high pixel counts appear both luminance side, so range for EMPeaks fitting is determined for luminance 20–220. Pixel counts outside the fitting range are shown in blue plots and within the fitting range are shown in red plots. Two narrow peaks and one broad peak, totally three peaks appear in the middle luminance range. (c) Low luminance side mapping. It shows outside the viewport. (d) High luminance side mapping. It indicates saturated luminance zone due to too bright diffraction spots.

side was excluded from the fitting range because it was saturated, but it is thought that more information can be taken in by adjusting the shooting parameters appropriately, and the number of peaks may change to four or much more.

The results of peak fitting for the first and 375th images (first image & last image) are shown in Figure 3. The peaks from the low-luminance side are called Peak1, 2, and 3. Mapping the intensity ratios of Peaks 1, 2, and 3 back to the original images with Equation(1). Specifically, the intensity of each peak was normalized by the sum of the three peaks to allow for a quantitative comparison of their relative proportions. In terms of the mapping calculation method, the ratio of each Peak at luminance X can be obtained by the following equation.

$$\text{Peak1_intensity_ratio(X)} = \frac{\text{Peak1_intensity(X)}}{\text{Peak1_intensity(X)} + \text{Peak2_intensity(X)} + \text{Peak3_intensity(X)}} \quad (1)$$

The above formula gives the Peak1_intensity_ratio (X) for a pixel with luminance X in the RHEED source image. Peak1 is mapped to the source image by doing so for all luminance X = 20 ~ 220. Similarly, Peak2_intensity_ratio(X) and Peak3_intensity_ratio (X) was calculated for Peak2 and Peak3 for all luminance X = 20 ~ 220 and mapped to the source image. In principle, Peak0_intensity_ratio always takes the value 0 ~ 1. Figure 3(c–e) show the intensity maps of each peak component (Peaks 1–3). The colored regions represent the information contained in each component. Figure 3(c), corresponding to Peak 1, shows generally higher intensity (darker color) in the lower region near the edge of the RHEED screen, which can be interpreted as reflecting background contributions. Figure 3(d), corresponding to Peak 2, exhibits regions where the diffraction spots appear suppressed (white), while higher intensity is observed around the central area of the RHEED screen and in regions where Kikuchi patterns are visible. In Figure 3(e), corresponding to Peak 3, the diffraction pattern itself is highlighted, making it the only component among the three in which the diffraction features are clearly represented. The peak fitting and mapping results for all images are shown in Supplement as movies. Since the trend remains the same across all images, we reinterpreted the original histograms (Figure 4), and found that, starting from the lowest intensity, we have Background 1 (Low-intensity inelastic scattered electrons) outside the viewport, a Background 2 (Low-intensity inelastic scattered electrons, Low-intensity Kikuchi pattern), the main part of the diffraction pattern (Elastic scattered electrons, High-intensity inelastic scattered electrons, High-intensity inelastic Elastic scattered electrons, High-intensity inelastic scattered electrons, High-intensity Kikuchi pattern), and saturated-

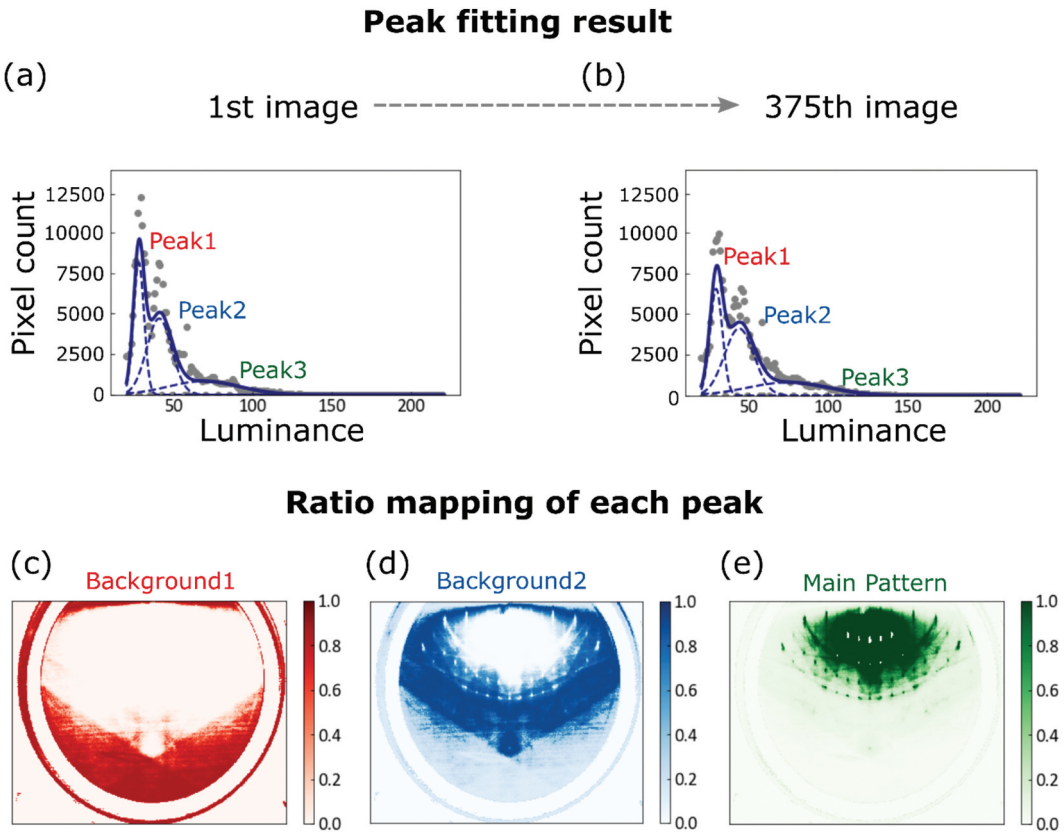


Figure 3. Results of peak fitting (a,b) peak fitting result with luminance histogram of 1st image and 375th (last) image. The tendency to exist two sharp peaks (Peak1 and Peak2) and a gentle peak (Peak3) from the low-luminance side remains the same throughout all images. (c–e) Peak ratio mappings of 375th (last) image. Peak 1 and 2 are background components and peak 3 contains the main diffraction pattern.

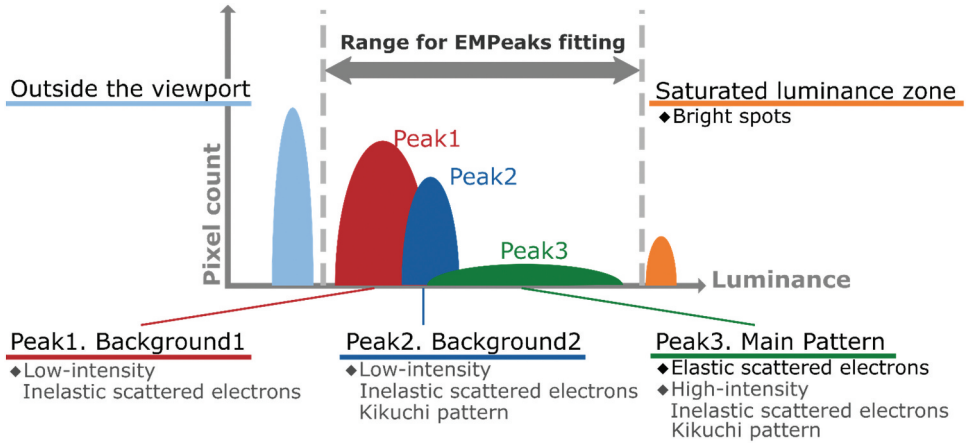


Figure 4. Conceptual diagram of interpretation to the entire luminance histogram. From low luminance side, five components are interpreted as the outside the viewport, background 1 (Low-intensity inelastic scattered electrons), background 2 (Low-intensity inelastic scattered electrons, Low-intensity Kikuchi pattern), main pattern (elastic scattered electrons, high-intensity inelastic scattered electrons, high-intensity Kikuchi pattern), saturated luminance zone (bright diffraction spots).

luminance zone (bright spots). Since we want to obtain information about surface structural changes by RHEED observation, we should focus on the Peak3, main pattern including diffraction information by elastic scattering and the brightness saturated-luminance zone.

In this way, although it is necessary for the researcher to interpret the peak ratio mapping to determine what physical information each component reflects, the present approach can be regarded as a 'white-box' analysis in which the meaning of the results is readily interpretable. At present, the number of peak components is determined empirically based on the histogram. However, for other materials, the number of components is not necessarily limited to three. To improve the general applicability of the

method, it would be desirable to enable automatic estimation of the number of components. One possible approach is to introduce maximum a posteriori (MAP) estimation based on Bayesian inference, as proposed in Ref [29], which we plan to explore in future work.

Figure 5(a,b) shows a time-series change of the luminance sum in the saturated-luminance zone and the Peak3 deviation σ. In counting the sum of luminance in saturated-luminance zone, the printed part of the date and time information of the camera was excluded. From Figure 5, it is clear that there are some extreme values and slope trends that change, assisting the points to focus on in the surface structure change (A–E). By looking back at the original images and interpreting each of them, we were able to estimate the optimal deposition time to create the $\sqrt{3}\times\sqrt{3}$, $\sqrt{31}\times\sqrt{31}$, and 4×1 structures, respectively (Table 1). Changes in external parameters such as time to stop deposition and time to stop heating could also be estimated, consistent with the conditions of the experimental procedure.

Other parameters (peak centers of Peak1 ~ 3 (μ), deviation (σ), and mixing ratio (π)) are shown in Figure 6. Among the three peaks, the deviation changed the most suggesting the possibility of detecting structure-related changes. It is considered that this is because the deviation is affected by all the changes in position, height, and area of Peak 3 caused by changes in the diffraction pattern, assuming that the number of incident electrons does not change much in principle. For α point, this point was interpreted as the moment when the balance between the collapse of the 7×7 structure and the generation of $\sqrt{3}\times\sqrt{3}$ changes. When 7×7 structure collapses, the spots become dim, so the deviation increases in terms of luminance distribution, but according to $\sqrt{3}\times\sqrt{3}$ structure generation, and smaller number of spots will appear, so the deviation becomes small again. Thus, α point is considered to be the time at which the balance changes from a 7×7 structure collapses to a $\sqrt{3}\times\sqrt{3}$ configuration. However, the change in the surface superstructure occurs gradually within the RHEED spot range, making it difficult to define the point of structural change fundamentally. Therefore, we treat α point only as the time where the balance changes from a collapsed 7×7 structure to a $\sqrt{3}\times\sqrt{3}$ configuration. The β point was interpreted as the moment when the balance between the collapse of the $\sqrt{31}\times\sqrt{31}$ structure and the generation of 4×1 changes. The $\sqrt{31}\times\sqrt{31}$ structural pattern has lots of spots and is fuzzy, so the deviation is large. In order to change to the 4×1 structure, the number of spots decreases and brightness is concentrated, which is expected to cause a decrease in dispersion, and in fact, it is a monotonous decrease. In addition, since there is no discontinuity between Peak 1 and Peak 2 at this β point parameters time series change, background changes such as fluctuations in the electron beam are not occurring. Considering the above, this point is considered to be the point where the change from $\sqrt{31}\times\sqrt{31}$ to 4×1 structure reconstruction is rapid and the moment when the balance between the disappearing of the $\sqrt{31}\times\sqrt{31}$ structure and the creation of the 4×1 structure changes, similarly to the α point. The γ point, the mixing ratio of Peak 1 and Peak 2 shows that a discontinuity change occurred at the same time as the discontinuity point of Peak 3, and the original image shows that the background became brighter. Therefore, it is thought that the intensity of

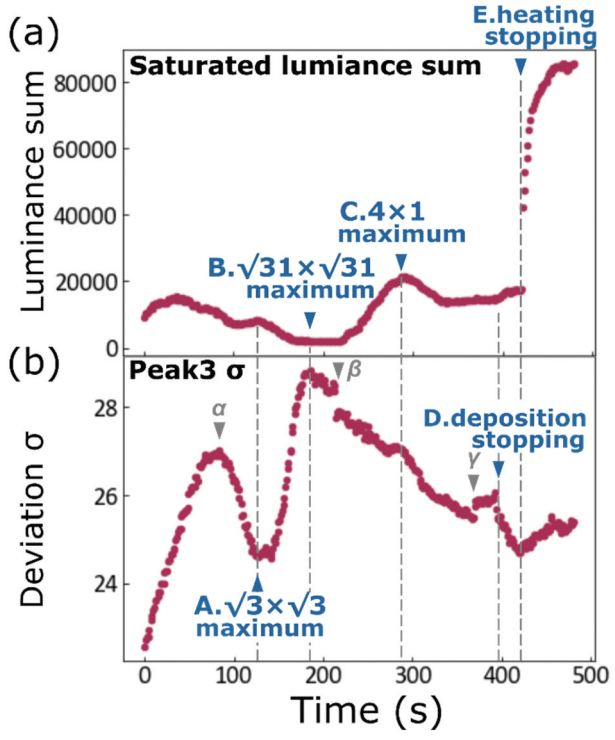


Figure 5. Time series change of two parameters. (a) Luminance sum of saturated luminance zone. (b) Peak33 deviation (σ). By focusing and interpreting the time when the parameters take an extreme value or change slope (point: A–E), optimal deposition time for fabricating each surface superstructure and the time when external parameter changed (i.e. deposition stopping, heating stopping) are estimated. The α point and the β point are considered change points originating from surface structural changes, and the γ point considered that originate from the increase in the incident electron beam. Details are in the main text.

Table 1. Time of focus (Figure 4. point: a–e) and interpretation of the event.

Point	Event	Time (s)
A	$\sqrt{3}\times\sqrt{3}$ structure intensity maximum	124 ~ 128
B	$\sqrt{31}\times\sqrt{31}$ structure intensity maximum	185 ~ 187
C	4×1 structure intensity maximum	287 ~ 290
D	Deposition stopping	392
E	Heating stopping	420

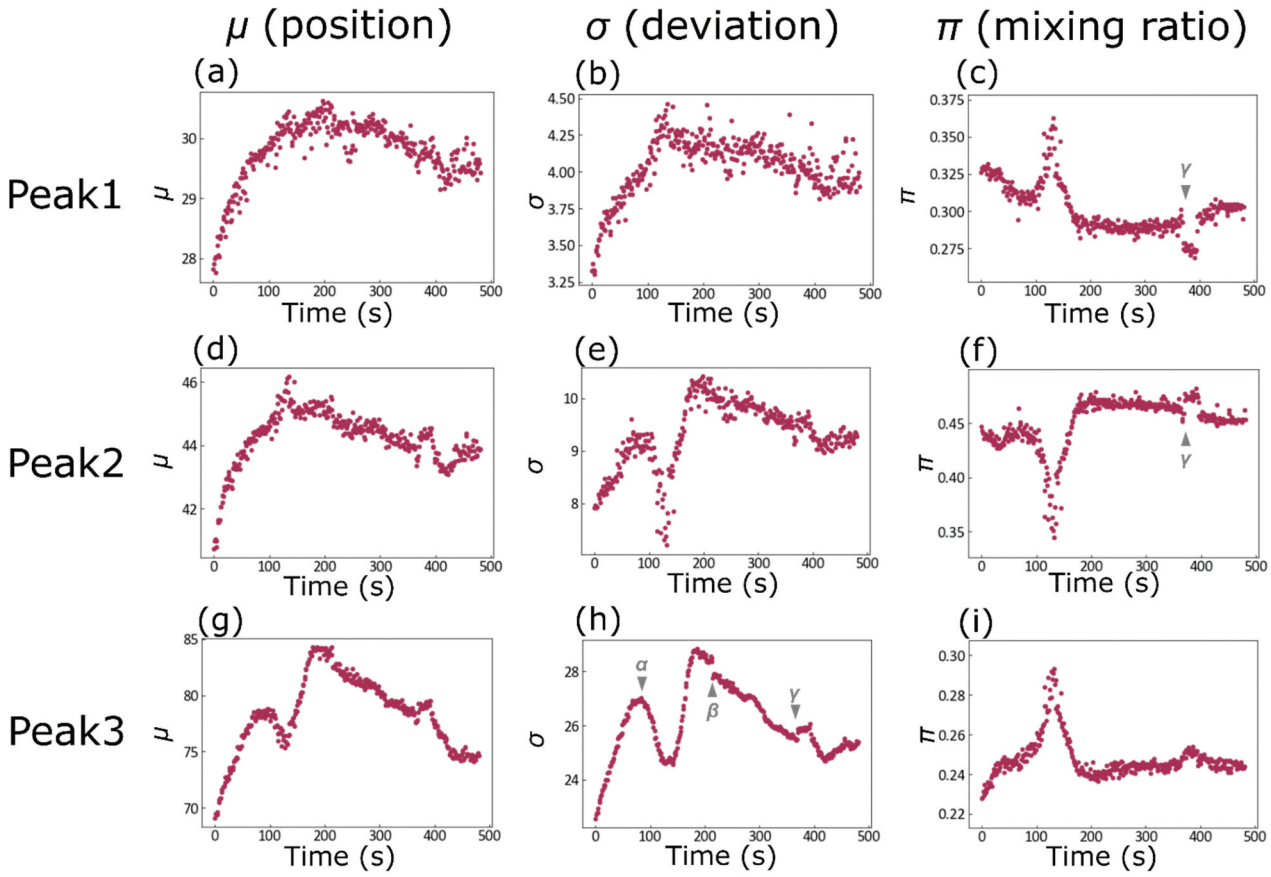


Figure 6. Change over time of all parameters for the three peaks.

the incident electron beam was increased. As shown in the interpretation of α-γ points, by considering the information of Peaks 1 and 2, it is possible to give an interpretation of the change point by considering whether the change is due to surface structure or external parameters such as electron beam and temperature changes.

To confirm the validity of the estimated optimal deposition time, we compared the estimated time results using non-negative matrix factorization (NMF) and using conventional method in our previous study [11], in Table 2. In the conventional method, experimenters should select the monitoring spot position or size in advance, so the estimated time is affected a lot depending on experimenters. Table 2 shows that the estimated time of proposed method agrees well with the NMF results and with conventional methods in previous studies, suggesting that it is useful as a method that can estimate the deposition time independent of the experimenter.

Table 2. Comparison of estimated optimal deposition time for fabricating each surface superstructure using EM peaks fitting, NMF [11], Conventional method [7–10].

Structure	EMPeaks Fitting (sec)	NMF (sec)	Conventional method (sec)
√3×√3	124 ~ 128	129	124 ~ 138
√31×√31	185 ~ 187	184	184 ~ 202
4 × 1	287 ~ 290	292	286 ~ 292

We also examined the robustness to image misalignment. As shown in Figure 7(a,b), the eighth image in the present image data showed an upward shift that it was hardly noticeable to the human eye. The one-dimensional array of luminance used in some RHEED machine learning analyses, including our previous study, only expands the image luminance to one dimension, and therefore, a completely different array is generated depending on the image shift. Therefore, when the 8th image was included in the analysis, it behaved as an outlier as shown in Figure 7 (c–e). Our analysis suggests that the proposed method exhibits a reasonable robustness in the analysis of the RHEED data analyzed in this study. However, a rigorous evaluation of robustness will require systematic testing using newly acquired datasets that include misalignments larger than that observed in the eighth frame. Such an evaluation will require the design of new experiments, together with an appropriate validation framework.

Furthermore, this method has the potential to be used for *in situ* analysis. Since this method performs converting image to luminance histogram and parameter extraction by peak fitting for each image, it has the potential for analysis while acquiring images of RHEED patterns. In this study, five EM fitting trials

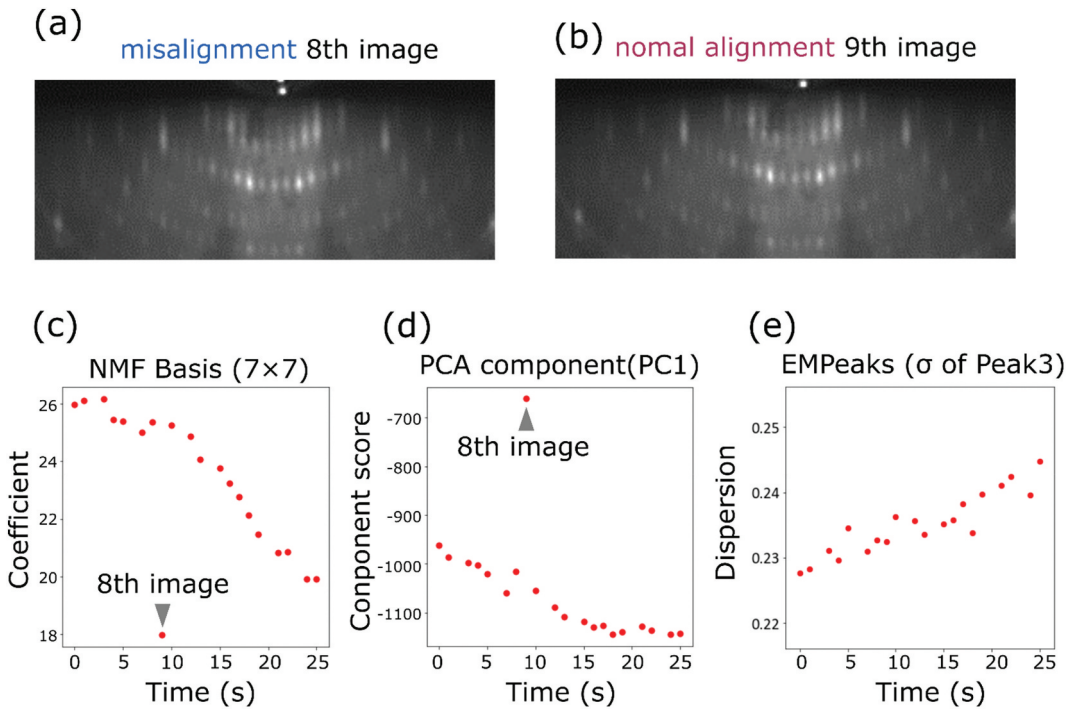


Figure 7. Comparison of robustness for image misalignment. (a, b) Crop parts of two images, (a) was 8th image, which was acquired with misalignment and (b) was 9th image which was acquired normally. (c–e) Comparison of time series results for extraction parameters near the 8th image using NMF, PCA, EMPeaks. When analyzing with 1-D luminance array, 8th image behaves like an outlier, but using luminance histogram and peak fitting using em peaks, 8th image behaves reasonably.

were executed for each histogram, and the total processing time was less than 1 s per image. Therefore, the calculation time is shorter than the interval between image acquisitions, and the possibility of application is expected to be sufficient. However, it is necessary to appropriately select the image acquisition interval and the number of peak fitting attempts per image for each experiment, depending on the combination of the desired accuracy of deposition rate and the computation time.

In the proposed method, the luminance histogram of a RHEED image is regarded as a spectrum, and by incorporating the peak fitting analysis technique, the information in the RHEED image can be divided into elements. By following the time series change of Peak3 and the saturated-luminance zone, assists were achieved in identifying the points to focus on, and estimation of the optimum deposition time for fabricating each structure and external parameters change time such as experimental conditions were succeeded. It is suggested that this method can be used for automatic analysis independent of the experimenter, while using information from the whole pattern and that there is a possibility of discovering features that have been overlooked until now.

The proposed method is advantageous for its high-throughput capability and the ability to extract latent features, such as background signal variations, independent of the operator's skill. In this study, the analysis was performed using single-domain RHEED images obtained from a vicinal substrate. It is anticipated that similar structural changes and optimal condition detection could also be achieved using multi-domain RHEED images obtained from a flat substrate. It is also expected to be used not only for surface superstructural changes, as in this study, but also for *in-situ* deposition rate confirmation of RHEED oscillations using all information of the RHEED pattern. However, future work is needed to address the possibility that the calculation results may fall into local solutions and to develop analytical methods that can retain quantitative information on the structure. The present results have suggested that the proposed method is reasonably robust to outliers and has potential applicability to RHEED data analysis. However, a rigorous validation of its applicability to RHEED data will require multiple independently acquired datasets obtained through new experiments, together with a validation framework to ensure reproducibility. Furthermore, a limitation is that spatial information, including lattice parameters, is discarded during the conversion to histograms. To address this, we propose a complementary approach: using the high-speed histogram analysis to precisely detect the timing of phase transitions, while referring to raw images for detailed crystallographic identification. This synergistic operation allows for both efficient real-time monitoring and accurate structural characterization. Looking ahead, since the method relies on luminance statistics rather than visual patterns, it suggests the potential for 'screenless' RHEED systems

using direct electron detection. Furthermore, its computational efficiency makes it suitable for autonomous experimentation, potentially offering a new perspective in the development of material fabrication processes.

3. Conclusion

In this study, we performed peak fitting analysis to luminance histograms of 375 RHEED images obtained during the process of indium deposition on Si(111) surface. Considering the out of fitting range elements and peak fitting result, the histograms are interpreted as being divided into five components: outside the viewport, background component1 (Low-intensity inelastic scattered electrons), background component 2 (Low-intensity inelastic scattered electrons), the main part of the diffraction pattern (Elastic scattered electrons, High-intensity inelastic scattered electrons, High-intensity Kikuchi pattern), saturated luminance zone. By focusing on the peak3 deviation (σ2) and pixel counts of the saturated luminance zone, the optimal deposition time for forming a specific surface superstructure can be automatically determined from time-series RHEED images of systems in which surface superstructures change with film thickness. By interpreting corresponding original RHEED image, the optimal deposition time for fabricating each surface superstructure and external parameter such as electron beam and temperature changes was estimated.

This method is more robust to image misalignment than the analysis using one-dimensional arrays of luminance and is expected to be used for *in-situ* analysis because our proposed method analyses each image one by one. As an automatic analysis method that uses entire information of RHEED images and does not depend on the experimenter's skill, this method is expected to be used to on-the-fly search for high-precision fabrication conditions for two-dimensional materials and to confirm the reproducibility of film growth.

Acknowledgements

We thank to Prof. F. Komori, Dr S. Tsuda, and Dr K. Yaji for useful discussions.

Disclosure statement

No potential conflict of interest was reported by the author(s).

Funding

This work was supported by JSPS KAKENHI Grant Number 23KJ1973 and JST PRESTO Grant Numbers JPMJPR20T7 and JPMJPR17NB. This work was also supported by JST CREST Grant Numbers JPMJCR21O4 and JPMJCR24A3, and JSPS KAKENHI Grant Numbers 21H04696, 25K01628 and 21H05012.

ORCID

Asako Yoshinari http://orcid.org/0000-0002-8049-5028
Yasunobu Ando http://orcid.org/0000-0003-3702-034X
Tarojiro Matsumura http://orcid.org/0000-0001-9950-509X
Masato Kotsugi http://orcid.org/0000-0002-4841-1808
Shuji Hasegawa http://orcid.org/0000-0002-6324-0525
Rei Hobara http://orcid.org/0009-0007-4449-6967
Naoka Nagamura http://orcid.org/0000-0002-7697-8983

Data availability statement

The data that support the findings of this study are available from the corresponding author upon reasonable request.

References

[1] Gupta A, Sakthivel T, Seal S. Recent development in 2D materials beyond graphene. Prog Mater Sci. 2015;73:44–126. doi: 10.1016/j.pmatsci.2015.02.002
[2] Novoselov KS, Geim AK, Morozov SV, et al. Electric field effect in atomically thin carbon films. Science (1979). 2004;306(5696):666–669. doi: 10.1126/science.1102896
[3] Wang S, Cui X, Jian C, et al. Stacking-engineered heterostructures in transition metal dichalcogenides. Adv Mater. 2021;33(16). doi: 10.1002/adma.202005735
[4] Lifshits VG, Saranin AA, Zotov AV. Surface phases on silicon: preparation, structures, and properties. Chichester: John Wiley & Sons; 1994.
[5] Abukawa T, Yamazaki T, Yajima K, et al. Weissenberg reflection high-energy electron diffraction for surface crystallography. Phys Rev Lett. 2006;97(24):245502. doi: 10.1103/PhysRevLett.97.245502
[6] Hasegawa S. Reflection high-energy electron diffraction. In: Kaufmann EN, editor. Characterization of materials. Hoboken, NJ: John Wiley & Sons, Inc; 2012. p. 1–14.
[7] Yamazaki S, Hosomura Y, Matsuda I, et al. Metallic transport in a monatomic layer of In on a silicon surface. Phys Rev Lett. 2011;106(11):116802. doi: 10.1103/PhysRevLett.106.116802
[8] Hasegawa S, Tong X, Takeda S, et al. Structures and electronic transport on silicon surfaces. Prog Surf Sci. 1999;60(5–8):89–257. doi: 10.1016/S0079-6816(99)00008-8
[9] Hasegawa S, Nagai Y, Oonishi T, et al. Structural phase transitions at clean and metal-covered Si(111) surfaces investigated by RHEED spot analysis. Phase Transitions. 1995;53(2–4):87–114. doi: 10.1080/01411599508200391
[10] Shibasaki T, Nagamura N, Hirahara T, et al. Phase transition temperatures determined by different experimental methods: si(111) 4×1-in surface with defects. Phys Rev B. 2010;81(3):035314. doi: 10.1103/PhysRevB.81.035314
[11] Yoshinari A, Iwasaki Y, Kotsugi M, et al. Skill-agnostic analysis of reflection high-energy electron diffraction patterns for Si(111) surface superstructures using machine learning. Sci Technol Adv

Mater. 2022;2(1):162–174. doi: 10.1080/27660400.2022.2079942
[12] Liang H, Stanev V, Kusne AG, et al. Application of machine learning to reflection high-energy electron diffraction images for automated structural phase mapping. Phys Rev Mater. 2022;6(6):063805. doi: 10.1103/PhysRevMaterials.6.063805
[13] Kwoen J, Arakawa Y. Classification of reflection high-energy electron diffraction pattern using machine learning. Cryst Growth Des. 2020;20(8):5289–5293. doi: 10.1021/acs.cgd.0c00506
[14] Provence SR, Thapa S, Paudel R, et al. Machine learning analysis of perovskite oxides grown by molecular beam epitaxy. Phys Rev Mater. 2020;4(8):083807. doi: 10.1103/PhysRevMaterials.4.083807
[15] Kaspar TC, Akers S, Sprueill HW, et al. Machine-learning-enabled on-the-fly analysis of RHEED patterns during thin film deposition by molecular beam epitaxy. J Vac Sci Technol A. 2025;43(3). doi: 10.1116/6.0004493
[16] Schmidt J, Marques MRG, Botti S, et al. Recent advances and applications of machine learning in solid-state materials science. NPJ Comput Mater. 2019;5(1):83. doi: 10.1038/s41524-019-0221-0
[17] Butler KT, Davies DW, Cartwright H, et al. Machine learning for molecular and materials science. Nature. 2018;559(7715):547–555. doi: 10.1038/s41586-018-0337-2
[18] Price CC, Li Y, Zhou G, et al. Predicting and accelerating nanomaterial synthesis using machine learning featurization. Nano Lett. 2024;24(46):14862–14867. doi: 10.1021/acs.nanolett.4c04500
[19] Shen C, Zhan W, Xin K, et al. Machine-learning-assisted and real-time-feedback-controlled growth of InAs/GaAs quantum dots. Nat Commun. 2024;15(1):2724. doi: 10.1038/s41467-024-47087-w
[20] Kim HJ, Chong M, Rhee TG, et al. Machine-learning-assisted analysis of transition metal dichalcogenide thin-film growth. Nano Converg. 2023;10(1):10. doi: 10.1186/s40580-023-00359-5
[21] Vasudevan RK, Tselev A, Baddorf AP, et al. Big-data reflection high energy electron diffraction analysis for understanding epitaxial film growth processes. ACS Nano. 2014;8(10):10899–10908. doi: 10.1021/nn504730n
[22] Bensaoula A, Malki HA, Kwari AM. The use of multilayer neural networks in material synthesis. IEEE Trans Semicond Manuf. 1998;11(3):421–431. doi: 10.1109/66.705377
[23] Lee KK, Brown T, Dagnall G, et al. Using neural networks to construct models of the molecular beam epitaxy process. IEEE Trans Semicond Manuf. 2000;13(1):34–45. doi: 10.1109/66.827338
[24] Gliebe K, Sehirlioglu A. Distinct thin film growth characteristics determined through comparative dimension reduction techniques. J Appl Phys. 2021;130(12). doi: 10.1063/5.0059655
[25] Harris SB, Gemperline PT, Rouleau CM, et al. Deep learning with reflection high-energy electron diffraction images to predict cation ratio in Sr2xTi2(1– x)o3 thin films. Nano Lett. 2025;25(14):5867–5874. doi: 10.1021/acs.nanolett.5c00787
[26] Matsumura T, Nagamura N, Akaho S, et al. Spectrum adapted expectation-maximization algorithm for high-throughput peak shift analysis. Sci Technol Adv Mater. 2019;20(1):733–745. doi: 10.1080/14686996.2019.1620123
[27] Matsumura T, Nagamura N, Akaho S, et al. Spectrum adapted expectation-conditional maximization algorithm for extending high–throughput peak separation method in XPS analysis. Sci Technol Adv Mater. 2021;1(1):45–55. doi: 10.1080/27660400.2021.1899449
[28] Matsumura T, Nagamura N, Akaho S, et al. High-throughput XPS spectrum modeling with autonomous background subtraction for 3 *d* 5/2 peak mapping of SnS. Sci Technol Adv Mater. 2023;3(1). doi: 10.1080/27660400.2022.2159753
[29] Matsumura T, Nagamura N, Akaho S, et al. Maximum a posteriori estimation for high-throughput peak fitting in X-ray photoelectron spectroscopy. Sci Technol Adv Mater. 2024;4(1). doi: 10.1080/27660400.2024.2373046
[30] Lifshits VG, Gavrilyuk YL, Saranin AA, et al. Surface phases on silicon. Phys Usp. 2000;43(5):525–527. doi: 10.1070/PU2000v043n05ABEH000754